ORIGINAL RESEARCH PAPER

Simulation of strong ground motion on near-fault rock outcrop for engineering purposes: the case of the city of Xanthi (northern Greece)

Z. Roumelioti[1] · A. Kiratzi[2] · B. Margaris[3] · A. Chatzipetros[2]

Abstract We combine probabilistic and deterministic approaches in an attempt to tackle a challenging topic in engineering seismology, that of the prediction of strong ground motion in urban areas located close to active faults, with sparse modern seismicity. The case we study is the city of Xanthi in northern Greece and we generate bedrock synthetic time series to be used as input motions into site-specific site effect analysis. We re-assess the seismic hazard using the probabilistic method and then perform hazard deaggregation in order to define realistic earthquake scenarios, which we examine in a deterministic way. The scenarios examined are: (a) a reference earthquake of M6.7, return period 100 years and at ∼30 km distance from the city and (b) a reference earthquake of M5.8, return period 475 years and at ∼3 km distance from the city of Xanthi. To compute synthetic time series for the distant source, we apply the stochastic method for finite faults. For the near-fault earthquake scenario we adopt a hybrid deterministic-stochastic approach that includes the semi-analytical method implemented in the COMPSYN code for the low frequency (∼<3 Hz) part of the spectrum and the stochastic method for the high-frequency (∼>3 Hz). The results of the probabilistic and the deterministic approaches converge to a satisfactory degree.

Keywords Deaggregation · Seismic hazard · Design motions

✉ A. Kiratzi
   kiratzi@geo.auth.gr

1   School of Civil Engineering, Aristotle University of Thessaloniki, Thessaloníki, Greece

2   Department of Geophysics, School of Geology, Aristotle University of Thessaloniki, 54124 Thessaloníki, Greece

3   Institute of Engineering Seismology and Earthquake Engineering [ITSAK-EPPO], Thessaloníki, Greece

1 Introduction

The objective of the present article is to provide estimates of broad band ground motions for rock outcrop in a moderate seismicity urban area in northern Greece, the city of Xanthi (Fig. 1). The city belongs to the Thrace Province, and the entire region, in terms of the Hellenic Building Regulation Code, belongs to Zone I, i.e., the zone of lowest design Peak Ground Acceleration (PGA = 0.16 g). Past seismic hazard studies in Greece have been presented at the national scale, always placing the town of Xanthi within the lowest seismic hazard zone, and very limited information exists on the regional scale (Margaris 1994). Even though the modern seismicity is moderate, Xanthi and other cities in Thrace have been severely affected by a series of earthquakes in the nineteenth century. Nowadays, gas pipe lines and the Egnatia Highway pass through the Thrace Province. They constitute vital horizontal infrastructure, not only for Greece but for other countries, as well.

Recent examples from the Aegean have taught us that even though most of the disastrous earthquakes tend to occur in well-known fault zones (as for example those of the Corinth Rift in central Greece and the Ionian Islands to the west; inset of Fig. 1), there are numerous examples of events which occurred in less known or unknown faults zones. These examples include the 1995, M6.6, Kozani and the 1999, M5.9, Athens earthquake sequences. In the aftermath of the occurrence of these events, the Greek national building code was modified to account for the increased level of possible ground motion at the respective regions. Another issue that raises concerns is our degree of knowledge of the geometry and the kinematics of all these faults that are included in the neotectonic maps, but which have no documented record of earthquakes and the instrumental data and field observations are not sufficient to define such characteristics.

In this work we attempt to address a number of these issues for the selected urban region. We re-assess the hazard after incorporating the most updated information on the possible hazardous earthquake sources and disaggregate the results to define realistic earthquake scenarios for different return periods. These scenarios are examined using
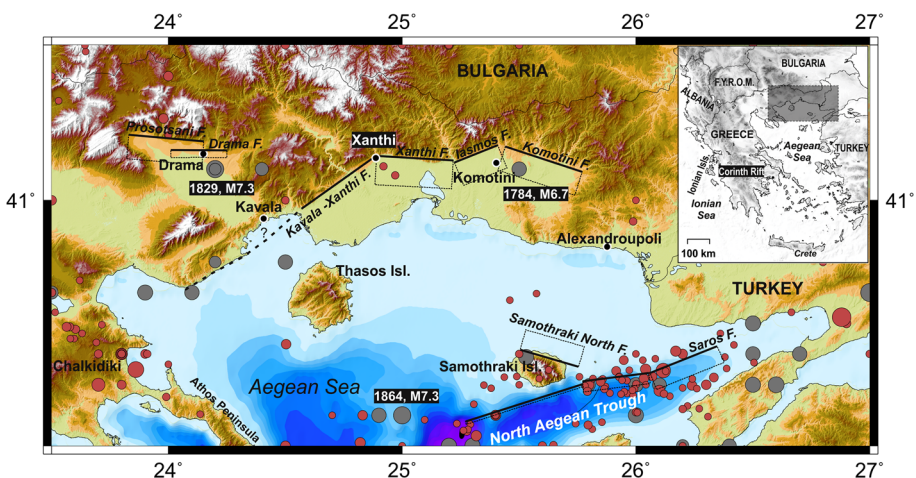

Fig. 1 Map of the broader study area showing the major faults (Caputo et al. 2012), all known (i.e., since 550 B.C.) historical (M ≥ 6.0; *gray circles*) and instrumental seismicity (M ≥ 4.0; *red circles*). *Inset* the broader area of Greece; *gray rectangular* denotes the zoomed area

purely stochastic or hybrid simulation methods, the exact method applied depending on the distance of the earthquake source from the urban area of Xanthi.

2 Seismicity and tectonic setting

Historical descriptions indicate that the city of Xanthi has been affected by the 1784 M6.7 earthquake near Komotini, but it was the 1829 series of earthquakes that totally ruined the city. More specifically, it was the 13 April 1829 earthquake that devastated Xanthi and its inhabitants (Ambraseys 2009; Papazachos and Papazachou 2003). Approximately one month later, on 5 May 1829, a M7.3 earthquake devastated the city of Drama (Fig. 1). The series of events culminated in 1864 with a M7+ event. The location of this earthquake is ambiguous; Papazachos and Papazachou (2003) place its epicentre in the North Aegean Sea (Fig. 1), while most of the damage has been reported in the Xanthi–Komotini basin. Instrumental data (available after 1900) show that the level of seismicity in the broader area is low-to-moderate, and that the most significant earthquakes occur along the North Aegean Trough (Fig. 1), which accommodates shear motions transferred from the North Anatolia Fault system, as it enters the Aegean Sea (Kiratzi 2014 and references therein).

Part of the aforementioned destructive seismicity has been attributed to the presumably active, more than 120 km long, Kavala–Xanthi–Komotini Fault Zone (KXK-FZ) (Caputo et al. 2012; Mountrakis and Tranos 2004; Sboras 2012), which is a south dipping tectonic structure, dominant feature in the area of study (Figs. 1, 2). From the geological and geomorphological point of view, the KXK-FZ defines the geological contact between bedrock to the north and sedimentary sequences to the south, and the boundary between the Rhodope mountain range and the alluvial plains of the Thrace basin (Mountrakis et al. 2006). Bedrock is comprised of metamorphosed rocks of the Rhodope Massif, a Palaeozoic-age complex of continental nature, consisted mainly of gneiss and marble (Fig. 2). Moreover, one of the most important geological units in the city of Xanthi is a granodiorite
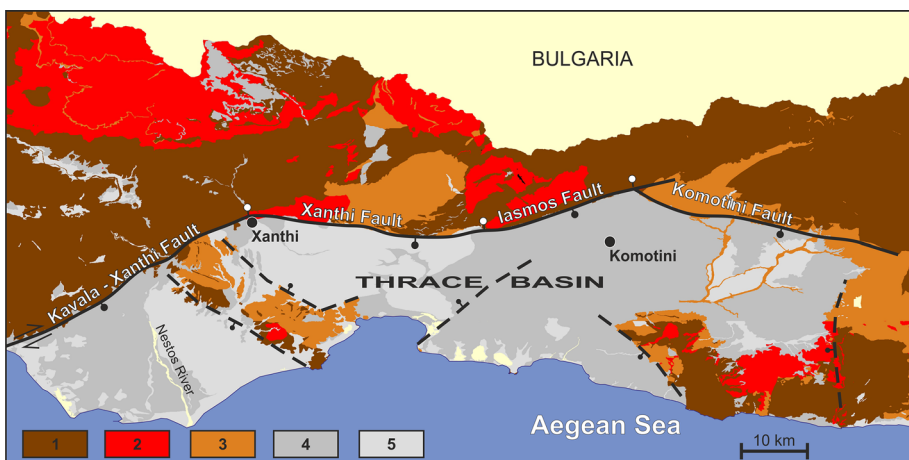

Fig. 2 Simplified geological map of the area of Xanthi, including the main fault zones described in the text. *1* Bedrock of the rhodope Massif, *2* Magmatic rocks, *3* Eocene and Oligocene sediments, *4* Neogene sediments, *5* Holocene sediments. Downthrown blocks are shown by *solid circles* and segment boundaries with *white* ones

intrusion, which dominates the footwall. The old part of the city is almost exclusively built on the granodiorite, while the newer parts are founded on the sedimentary cover of the basin. The KXK-Fault Zone is divided into four major segments of different orientation (Mountrakis et al. 2006), whereas the three eastern segments, e.g. the Xanthi, Iasmos and Komotini Faults (Figs. 1, 2) show evidence of recent activity (Caputo et al. 2012). These faults are the subject of our analysis, and from this point forward, we will refer to them as Thrace Fault Zone. The length of these segments ranges from ~15 to ~30 km. More segments could be identified toward the city of Kavala in the west, while the extension of the fault zone into the Gulf of Kavala is considered very probable (Martin 1987).

The greater urban region of Xanthi is spatially developed along the intersection of the Kavala–Xanthi fault with the Xanthi fault, and extends up to the intersection with the Iasmos fault (Fig. 1). The Xanthi fault scarp is oriented approximately E–W and extends for ~27 km from Xanthi up to the village of Iasmos, where it terminates against a NNW-SSE rectilinear fault (Mountrakis and Tranos 2004). The Iasmos fault scarp is more NE-SW oriented and its surface length is no more than 17 km. Field measurements and kinematic indicators denote that both fault segments dip at approximately 50° and that their dominant sense of movement is normal (e.g. Mountrakis and Tranos 2004; Mountrakis et al. 2006). Although this mainly normal sense of movement characterizes the most recent deformation phase of both segments, the entire fault zone probably initiated as a long strike-slip structure that caused the emplacement of Xanthi pluton (Koukouvelas and Pe-Piper 1991).

Despite the fact that no strong earthquake has been confidently associated with the Xanthi and Iasmos faults, the topographic relief across the range front of up to 1300 m indicates intense deformation during Quaternary times. This is supported by other observations, as for example the fast uplift of the footwall, documented at the deep incising of river meanders, the north facing backscarps on the plain. Holocene activity of the fault zone cannot be adequately supported, due to the lack of obvious geological and morphotectonic characteristics, such as faulting of alluvial fans. However, taking into account the zone's profound geomorphological signature and the fact that it is favorably oriented in respect to the active stress field, which implies ~N–S extension, it is characterized as a possibly active fault zone, prone to reactivation (Mountrakis and Tranos 2004).

3 Assessment and deaggregation of probabilistic seismic hazard

To define realistic earthquake scenarios for Xanthi, we initially performed a probabilistic seismic hazard analysis (PSHA) and subsequently disaggregated its results to examine the seismic hazard as a function of earthquake magnitude and distance from the possible rupture zones. The purpose of PSHA, in general, is to compute how often a specified level of ground motion will be exceeded at the site, taking into account the multiple seismic sources affecting it. The distinction between the ground motions from the sources for different magnitudes and distances are considered in the deaggregation process. A PSHA has the ability to, and should, merge all pieces of information available for the description of the seismic potential in an area. These include known or suspected occurrence of the seismic events in a "non-random" way in time, space and size; assumed (e.g., empirical proposed for other, similar seismotectonic environments) or ad-hoc (e.g., empirical, derived on the basis of region-specific data) models that describe the wave propagation in the earth crust; empirical or theoretical means of estimating the effect of the shallowest

geological formations on the amplitude and frequency content of the seismic wave field. Despite the ongoing debate on PSHA limitations (Frankel 2013a, b; Stein and Stirling 2015; Stein and Stein 2014), this method of assessing seismic hazard remains the most useful tool for seismologists and engineers when it comes to engineering design and decision-making on seismic hazard mitigation.

The first step in a typical PSHA includes the identification and geometrical description of all seismic sources—active faults capable of generating ground motions above a threshold level at the site of interest. In our analysis we combined and incorporated the pertinent results of several previous studies in the broader study area of the city of Xanthi. We adopted the seismotectonic model proposed by Papazachos et al. (2001) consisting 159 active seismic faults (Fig. 3; black thick lines), complimentary to the seismic sources (Papaioannou and Papazachos 2000) of the broader region (Fig. 3; shaded areas). Finally, the Greek Database of Seismogenic Sources—GreDaSS (Caputo et al. 2012) was used to describe the Thrace Fault Zone.

The next step in the classical PSHA analysis includes the characterization of the distribution of earthquake magnitudes, i.e. the rates at which earthquakes of different magnitudes are expected to occur. We adopted the rates provided by Papazachos et al. (2001) for the seismic faults, based on historical and instrumental data for strong earthquakes (M ≥ 6), together with the relative rates for the seismic sources by Papaioannou and Papazachos (2000). We had to make assumptions for the seismicity rate of the Thrace Fault Zone, which, as mentioned earlier, has been recognized as a significant neotectonic structure (Caputo et al. 2012 and information presented in this work), but it has not been clearly related to specific seismic activity during historical and instrumental times. In our analysis, we decided to test two quite different annual rates of seismic activity, r = 0.004 and r = 0.007, based on the available information for neighbouring seismic faults (Papazachos et al. 2001).
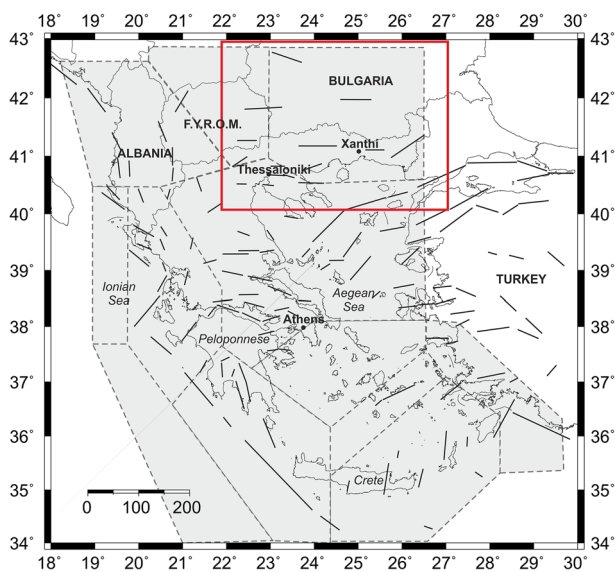

Fig. 3 Line (*black thick lines*) and area (*shaded polygons*) seismic sources used as input in the probabilistic seismic hazard analysis (PSHA) for the target area included within the *red rectangle*

Having defined the potential seismic sources, earthquake magnitudes and source-to-site distances, a suitable equation to predict the values of the examined ground motion intensity measure as a function of magnitude and distance, is required. As the intensity measure we selected the Peak Ground Acceleration (PGA), and as suitable Ground Motion Prediction Equation (GMPE) we used that of Skarlatoudis et al. (2003, 2007), which is based on Greek strong motion data.

The last step of the analysis refers to the calculation of the earthquake activity rate, at which PGA amplitude exceeds certain thresholds, for each seismic source (either linear or area). These rates are taken as the expected probabilities to generate motions of such amplitude, in order to assess the hazard. Our analysis is combining uncertainties in earthquake magnitudes, in source-to-site distances and in the amplitudes of the PGA, defined empirically. For this purpose we used the FRISK88M software (Risk Engineering 1995) incorporating various return periods (probabilities of exceedances), i.e., T_R = 50, 100, 200, 475, 950 years. The results of the PSHA for these periods and the PGA (in cm/s^2), assuming surface geological conditions of rock, are presented in Table 1. Results are shown for both tested values of the seismicity rate of the Thrace Fault Zone. It is interesting to note that the PGA value corresponding to T_R = 475 years is much larger compared to the design PGA value indicated for the broader area in the national building code (0.16 g). Such a discrepancy is expected for several reasons. Except from differences in the PSHA analysis itself (different source representation, GMPE etc.), the primary reason for such a discrepancy is the fact that the national code design value is referred to a wide area (zone), while our results are specific for the town of Xanthi, which is located next to an active (at T_R = 475 years) fault. Furthermore, the PGA design values provided in the Hellenic Building Regulation Code are "effective" PGA values, i.e., values that have been empirically trimmed by a certain percentage (usually 20 %, although the exact percentage has not been officially documented). In Fig. 4, we compare our results to corresponding results from the previous work of Margaris (1994). In the latter, PSHA was performed for the broader area of northern Greece using a seismic source model consisting of 6 area sources. In general, herein results are quite close to those of the previous assessment, considering the differences in the modelling of the potential seismic sources and the adopted GMPEs.

Following the PSHA, we performed deaggregation of the seismic hazard by magnitude, distance and ground motion epsilon. The basic advantage of the PSHA is that it integrates the hazard to an examined site from all contributing seismic sources. However, this advantage is also a disadvantage in cases when there is the need to isolate a specific earthquake scenario, as for example in studies that require time series of strong ground motion measures. The application of seismic hazard deaggregation allows us to determine which earthquake source, magnitude and distance contributes mostly to the overall seismic

Table 1 Probabilistic seismic hazard analysis (PSHA) results (for PGA $\pm 1\sigma$) for different values of the return period, T_R, and the activity rate, r, of the Xanthi fault, which is the closest known potential earthquake source for the city of Xanthi

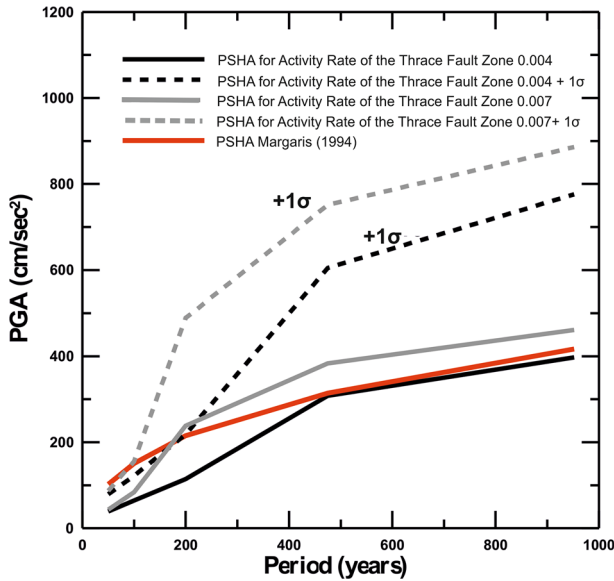|	T_R (years)				
	50	100	200	475	950
PGA (cm/s^2) $\pm 1\sigma$ r = 0.004/year	39 ± 40	64 ± 58	115 ± 104	308 ± 297	398 ± 378
PGA (cm/s^2) $\pm 1\sigma$ r = 0.007/year	43 ± 44	84 ± 72	238 ± 251	384 ± 367	461 ± 425

Fig. 4 PGA's derived from the PSHA (+1 SD, σ; *dashed lines*) for the urban area of Xanthi as were derived for two different annual activity rates assumed for the Thrace Fault Zone; r = 0.004 (*black lines*) and r = 0.007 (*grey lines*). Corresponding results from previous work (Margaris 1994) are shown for comparison (*red*)

hazard at a site of interest. Deaggregation methods have been carried out by several researchers (e.g. Chapman 1995; Cramer and Petersen 1996; Harmsen 2001; McGuire 1995; Stepp et al. 1993). Here, we followed the suggestions and principles of the seminal work of Bazzurro and Cornel (1999).

As mentioned, we applied seismic hazard deaggregation which includes variability in earthquake magnitude, M, source-to site distance, D as well as ground motion uncertainty, ε, in order to account for aleatory variability. All these were performed within the modules of the HAZ30 software (Bazzurro and Abrahamson, *pers. comm.*) taking into consideration the output of FRISK88M code. We decided to be on the more conservative side and adopted the PSHA results that correspond to the value of activity rate of 0.007 for the

Table 2 Seismic hazard deaggregation results at the centre of the city of Xanthi for different values of the return period, T_R

	T_R (years)				
	50	100	200	475	952
PGA (cm/s^2)	43	84	238	384	461
M	6	6.7	7.3	5.8	5.9
D	33	33	29	3	3
ε	0.19	0.31	0.56	0.94	0.94

M is for earthquake magnitude, D for distance and ε the standard deviation from the median ground motion as predicted by a GMPE

Thrace Fault Zone. Results of this analysis indicate the relative contribution of the examined seismic sources in the (D, M, ε) bin. The tested magnitude-bin width was 0.1 and the corresponding distance-bin width was 2 km, relatively short as the area of interest was not very large. The deaggregation analysis identified the earthquakes having the largest contribution to the estimated hazard for the urban area of Xanthi, and, as expected, these earthquakes differ for each of the different examined return periods (Table 2). For return periods of 50, 100 and 200 years, earthquakes from sources at distances of the order of 30 km dominate the hazard, while at larger return periods, i.e. 475 and 950 years, the most hazardous earthquake source is the Xanthi fault, i.e. the closest mapped neotectonic fault. Estimated PGA range from 43 cm/s^2, for the return period of 50 years, to reach 461 cm/s^2
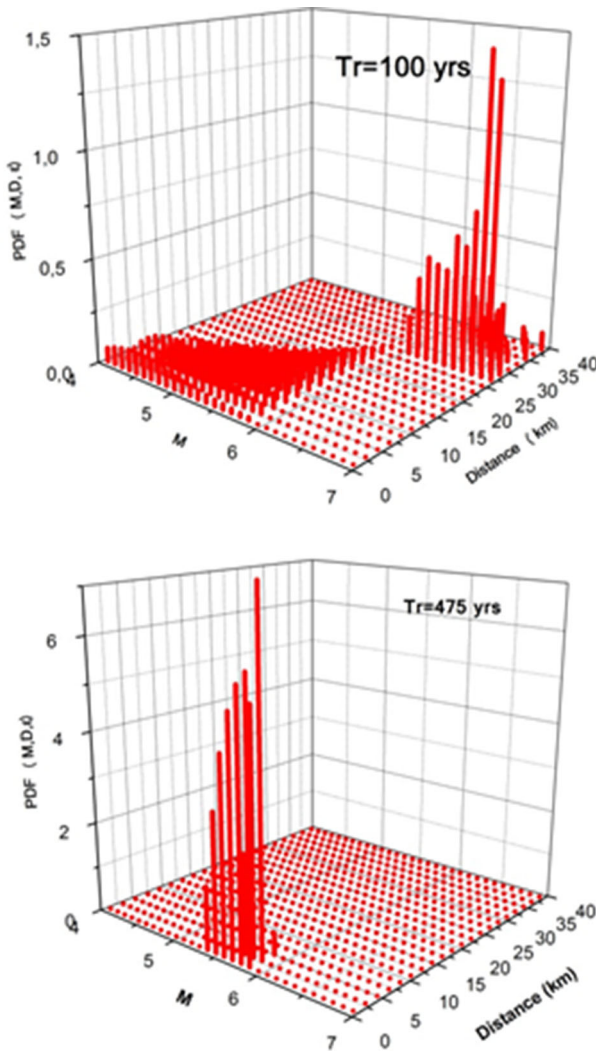

Fig. 5 Results of the deaggregation analysis of the probabilistic seismic hazard for the town of Xanthi for the return periods of 100 years (*top*) and 475 years (*bottom*)

for the largest return period examined (950 years). We indicatively present the results of the deaggregation analysis for the return periods of 100 and 475 years in Fig. 5.

4 Ground motion simulations for the city of Xanthi

To estimate the expected level of ground shaking, we selected two reference scenarios, highlighted by the deaggregation analysis, one relatively distant and one close to the city of Xanthi. We analyse a scenario earthquake of M6.7 on the Komotini fault, at a distance of 33 km from Xanthi (T_R = 100 years) and a scenario earthquake of M5.8 on the Xanthi fault, at the close distance of 3 km from Xanthi (T_R = 475 years). The former scenario is placed at the seismogenic source that has been related to the M7.3 earthquake of 1864 (Papazachos and Papazachou 1997, 2003). The Xanthi fault, as discussed earlier, has not been unambiguously related to any destructive past event, although many scientists favour its relation to the April 1829, M6.6 earthquake, that preceded the catastrophic May 1829 M7.3 Drama earthquake.

4.1 Scenario earthquake M6.7 on the Komotini fault (for T_R = 100 years)

4.1.1 Method

To investigate the more distant M6.7 on the Komotini fault earthquake scenario, we chose to apply the stochastic method for finite faults. The stochastic method was originally proposed by Boore (1983) and lies amongst the most commonly used tools from engineers and seismologists when it comes to simulating strong ground motion from earthquakes. The original method was extended by Beresnev and Atkinson (1997) to incorporate the finite dimensions of seismic sources and Motazedian and Atkinson (2005) released the EXSIM code, which further advanced the stochastic method by replacing the static subfault corner frequency, of previous implementations of the method, by a dynamic corner frequency. This dynamic corner frequency is related to the dimensions of the area that experiences slip at a certain point in time during the rupture process of an earthquake. EXSIM also incorporated the analytical model of Mavroeidis and Papageorgiou (2003) that can simulate long-period pulses, often observed in the near-field of an earthquake. The most recent version of EXSIM was based on the publication of Boore (2009) and is the one adopted for the herein presented stochastic simulations.

The stochastic method, both in its original form and after its modifications, has been repetitively applied and validated in various seismotectonic environments around the globe (Boore 2009 and references therein). It has also been adopted in several studies of earthquakes in the broader Aegean area (e.g. Benetatos and Kiratzi 2004; Karastathis et al. 2010; Margaris and Boore 1998; Mountrakis et al. 2012; Roumelioti et al. 2004; Theodulidis et al. 2006) and is considered as an effective tool, especially in cases where the sparsity of seismological data does not facilitate the application of more refined and physically sound methods.

In brief, in the stochastic method for finite faults the seismic source is modelled as a rectangular plane, divided into a certain number of subfaults, each of which is then treated as a point source. Each point source is assumed to radiate seismic energy described by a simple theoretical seismological model such as the ω^{-2} model (Brune 1970, 1971) adopted herein. Seismic waves are empirically attenuated from the centre of each subfault to the

observation point at the ground surface, where they are summed with proper time delays to produce the synthetic ground motion time history. That is to say that waves generated at the source are not propagated through a specific velocity model, but are attenuated through empirical relations that describe anelastic attenuation and geometric spreading in the broader area of interest. Site effects can be grossly encountered through the use of frequency-dependent empirical amplification factors. For a detailed description of the stochastic method, the reader is referred to the work of Boore (1983, 2003, 2009), Beresnev and Atkinson (1997) and Motazedian and Atkinson (2005).

4.1.2 Application and results

The geometry of the considered seismic source, the seismic wave propagation path effect and the site effect at the observation point(s), input parameters of the stochastic method are summarized in Table 3. The Komotini fault has a surface length of 29 km (Fig. 1) and it has the potential to produce earthquakes as large as 6.7 (Caputo et al. 2012). We modelled this fault by a rectangular plane of dimensions 29 km × 14 km, which was discretized in 18 × 9 subfaults. The top edge of the fault model was placed at 0 km, based on our experience that events of M6.7 are expected to have slip patterns that reach the earth's surface.

The propagation model includes parameters for the geometric spreading, the anelastic attenuation, and the near-surface attenuation, as well as site-amplification factors. For the

Table 3 Modelling parameters for the application of the finite-fault stochastic method in the investigation of the scenario earthquake of M6.7 on the Komotini fault

Parameter	Symbol	Value
Fault orientation	ϕ_1	Strike 90°
	δ_1	Dip 56°
Fault dimensions	L	Length 29 km
	w	Width 14 km
Depth of upper edge of fault	h	0.0 km
Seismic moment magnitude	M_w	6.7
Stress parameter	Stress	56 bars
Number of subfaults (along strike × along dip)	$N_L \times N_W$	18 × 9
Subfault including the Hypocentre	i_0, j_0	Random
Crustal shear-wave velocity	β	3.4 km/s
Crustal density at source depth	ρ	2.7 g/cm^3
Geometric spreading as a function of distance, R (km)		1/R
Source duration	T_S	1/f_{0s}, f_{0s} being the subfault corner frequency
Path duration ($T_P = bR$)	T_P	b = 0, $R < 10$ km; b = 0.16, $10 \leq R \leq 70$ km (Atkinson and Boore 1995)
Anelastic attenuation model, Q(f) = Q_0*f**eta	Q_0	88.0
	η	0.9
Kappa	κ_0	0.035 s
Site amplification empirical factors	A(f)	Klimis et al. (2006) (Table 4)

geometric attenuation we applied a geometric spreading operator of 1/R, and the anelastic attenuation was represented by a mean frequency–dependent quality factor, (Hatzidimitriou 1993, 1995), derived from studies of S-wave and coda-wave attenuation in northern Greece.

To account for the near-surface attenuation at high frequencies, we diminished the simulated acceleration spectral amplitudes by the factor $\exp(-\pi\kappa f)$ (Anderson and Hough 1984). The spectral decay factor kappa (κ) was given the value 0.035 which corresponds to rock site conditions (Margaris and Boore 1998). Simulations were performed assuming surface geological conditions of hard rock, which were incorporated through appropriate empirical amplification factors suggested by Klimis et al. (2006) (Table 4).

Due to the distance of the considered seismic source and the small area of the city of Xanthi, simulated time histories showed negligible variation within the city limits. As an example, the simulated acceleration time history, at the centre of Xanthi, from the scenario earthquake of M6.7 on the Komotini fault, along with its pseudo-acceleration response spectrum (5 % damped) are presented in Fig. 6. Results refer to the S-wave part of the ground motion at a random horizontal direction. The duration of strong ground motion is circa 15 s, while PGA is estimated at 67 cm/s^2, a value that is in good agreement with the results of the PSHA for the return period of 100 years (at -0.2 to 0.3 σ of the mean PGA value for r = 0.007/year and really close to the value of 64 cm/s^2 when r = 0.004/year) (Table 1). The estimated level of strong ground motion throughout the entire simulated range of frequencies is well below the current design levels of both the national building code and EC8, although site and other effects (source directivity, topographic, etc.) that may significantly alter the characteristics of ground motion are the subject of another study.

4.2 Scenario earthquake M5.8 on the Xanthi fault (for T_R = 475 years)

4.2.1 Method

The proximity of the M5.8 earthquake scenario to the city of Xanthi (source-to-site distance ~ 3 km) imposed the use of a different method compared to the one adopted for the investigation of the more distant earthquake scenario on the Komotini fault. Rupture of the close-by Xanthi fault would most probably trigger near-source effects that would result to considerable ground motion variability, even within the limited extent of the city of Xanthi. Such phenomena are primarily deterministic and, thus, we chose to simulate them using a semi-analytical method. On the other hand, even in the near-source region of an earthquake, high frequencies of the seismic spectrum remain incoherent and of stochastic character and can be adequately simulated using the afore-described finite-faults stochastic simulation method. So, the resulting synthetic ground motions was decided to be the hybrid result of a deterministic approach for the simulation of the low-frequency part of the seismic spectrum and of a stochastic approach for the simulation of higher frequencies.

To theoretically simulate large-period ground motion from the close-by, to the site of interest, rupture scenario we applied the semi-analytical method of Spudich and Xu (2003). The specific method, implemented in the code COMPSYN, presents several advantages against other widely used methods such as the stochastic, finite and spectral elements (Douglas and Aochi 2008). It is mathematically accurate for a quite wide range of frequencies, which is user defined. Green's functions are calculated to include the complete response of the adopted 1D velocity structure i.e. P and S waves, surface waves, near-field terms and leaky modes. At the same time, the method is quite fast in its application. The
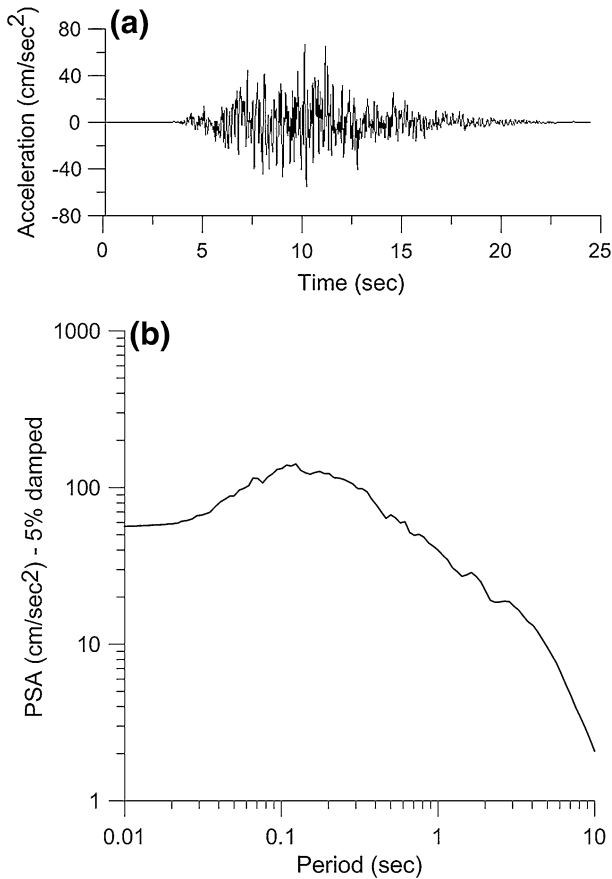
Fig. 6 **a** Simulated acceleration time series and **b** 5 %-damped pseudo-acceleration response spectrum, at the center of Xanthi, as derived using the finite-fault stochastic method for the scenario earthquake of M6.7 on the Komotini fault

basic disadvantage, however, being that it does not take into account the anelastic attenuation of seismic waves and, thus, its results are reliable up to a distance beyond which this phenomenon is considerable (e.g. 40–50 km from the seismic source; Street et al. 1975). In the case of the herein examined earthquake scenario this does not comprise a problem since source-to-site distances do not exceed 20 km.

COMPSYN uses the methodology of Spudich and Archuleta (1987) to evaluate the representation theorem integral onto the assumed fault surface. Green's functions describing the unit response of the vertically varying, laterally homogeneous velocity structure are calculated by the discrete-wavenumber finite-element method of Olson et al. (1984). They are computed at the observation points' locations as tractions on the fault model plane, using the reciprocity theorem. Then the user-defined kinematic fault model characteristics are taken into account to perform the convolution between slip and the Green's functions and to integrate the result over the entire fault surface to produce the spectra of ground motion at the simulation sites. Finally, synthetic Fourier spectra are inverse transformed to provide the corresponding synthetic time histories.

COMPSYN has been widely used by engineers and seismologists in both research and practical applications in various areas of the world (Douglas and Aochi 2008 and references therein), its use in Greece has been quite limited. To our knowledge there is just one relative publication in which COMPSYN has been applied to provide blind predictions of strong ground motion from scenario earthquakes for the city of Thessaloniki (Ameri et al. 2008). In our area of interest, i.e. the broader area of Xanthi, there are no records of previous earthquakes, not even from a moderate-magnitude one, to validate any simulation method. As an alternative solution we decided to validate the COMPSYN code in one recent event that occurred in Peloponnese, southern Greece, on June 08, 2008 M6.7. A description of this application, which resulted in quite successful simulations of the observed strong ground motion records, is presented in the Supplement.

4.2.2 Application and results

According to Caputo et al. (2012), Xanthi fault is mapped with a surface trace of 27.5 km length, i.e. capable of producing events of much larger magnitude compared to the one examined herein. The dimensions of the fault model for the M5.8 earthquake scenario were selected based on the empirical relations of Wells and Coppersmith (1994) (Fig. 7). The depth of the upper edge of the fault model was placed at 3 km based on experience from previous earthquakes of similar magnitude and rupture kinematics in Greece. We examined an average scenario, in terms of rupture directivity, where the rupture initiation point is placed at the deepest, central part of the assumed fault surface and the slip distribution was computed following the methodology of Mai and Beroza (2003). In other words, we were not interested at this point to investigate ground motion variability related to variations of the source process or "worst" rupture scenarios including, for example, strong rupture directivity effects toward the observation sites.

Theoretical Green's functions were computed in the frequency range 0–4 Hz adopting the 1-D velocity model proposed by Papazachos (1998). We modified its shallowest part (0–1 km) in order the S-wave velocity to be 1.29 km/s at the ground surface, assuming rock outcrop surface geological conditions (Table 5). This was done to achieve
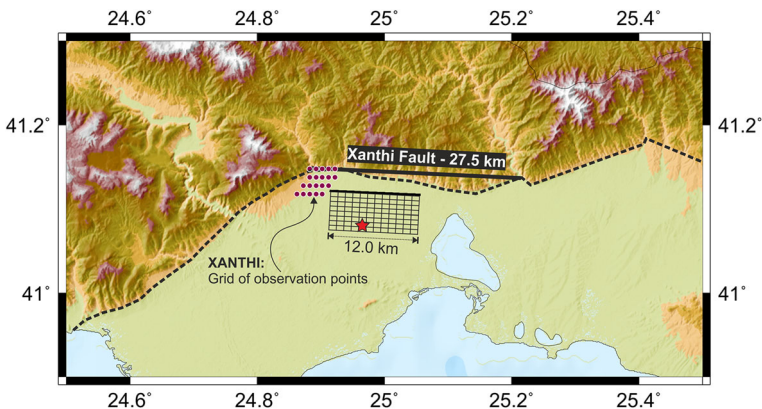

Fig. 7 Geometry of the segment of the Xanthi Fault modelled in the scenario earthquake. The projection of the fault model discretised in 1×1 km^2, is shown at the centre, with its upper edge (*thick black line*) located at 3 km depth. The *star* denotes the adopted rupture initiation point (hypocentre). The grid of observation points to simulate ground motions at each node is marked with *circles*

Table 4 Empirical site amplification factors for rock outcrop as suggested by Klimis et al. (2006)

Frequency (Hz)	Amplification factor
0.11	1.035
0.16	1.046
0.3	1.084
0.46	1.132
0.79	1.244
1.06	1.328
1.25	1.374
1.54	1.437
1.76	1.478
2.07	1.529
2.55	1.597
3.42	1.701
4.94	1.839
7.24	2.003
9.2	2.11
15.72	2.347
23.49	2.524
30.42	2.63
45.38	2.787

compatibility with the results of the extensive geotechnical studies conducted in the area (Kiratzi et al. 2013; Koskosidi 2014; Theodoulidis et al. 2014). The simulation points (20 in total) are nodes of a grid that covers the area of the city centre and its suburbs (Fig. 7).

The synthetic velocity time histories, are shown in Fig. 8a–c, for three components of ground motion, i.e. the fault-normal, the fault-parallel and the vertical. From a comparative examination of the relative amplitudes, we conclude that ground motion appears much larger on the fault-normal component, as it is theoretically expected. Along this direction, waveforms are dominated by a single long-period pulse, appearing one-sided or double-sided depending on the location of the observation point with respect to the causative fault. Variability is also observed in terms of the peak ground velocity (PGV), with the largest value surpassing 70 cm/s at the observation point that is closest to the fault (Fig. 8a, second row from bottom—rightmost plot). In general, peak values along the other two examined directions are 3–4 times lower. Vertical synthetic seismograms appear more enriched in high frequencies compared to the respective horizontal records, although they also show a long-period pulse at their early parts, signature of the near-fault effects.

The exact source model used in the deterministic simulations was inserted into a new round of simulations with the EXSIM code, which computes synthetic time histories at a random horizontal direction of ground motion. The input parameters adopted in the stochastic method are summarized in Table 6. The synthetic acceleration waveforms, computed at the 20 observation points, were integrated to velocity (Fig. 9). Even though EXSIM is applicable to a wide range of engineering interest frequencies (usually in 0.1–20 Hz), we only kept the time-series for frequencies above 2 Hz, since lower frequencies were earlier deterministically simulated. Synthetic PGA values at several grid points are of the order of 400 cm/s^2, i.e. close to the PGA value suggested by the PSHA analysis for the corresponding return period of 475 years (Table 1).
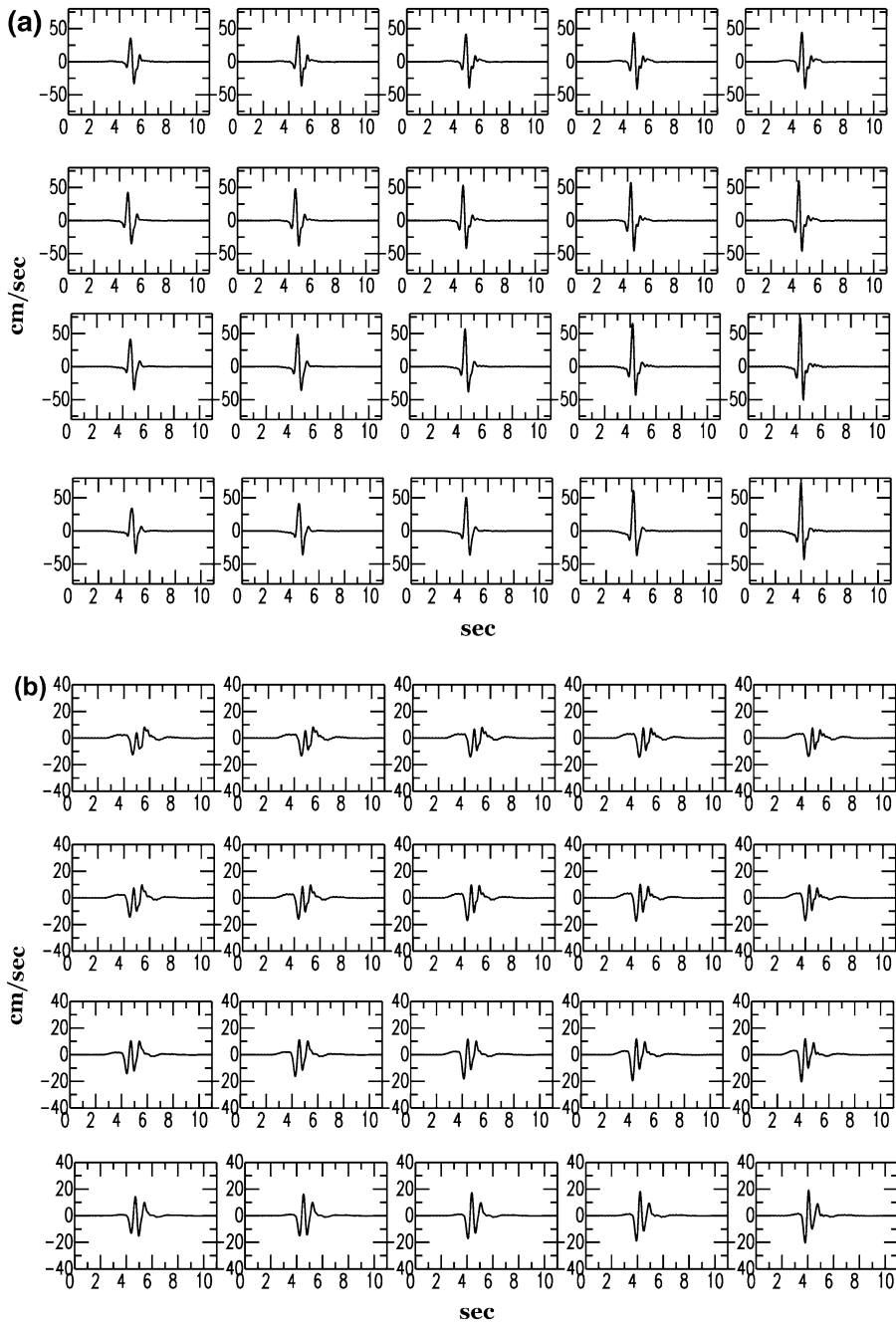
Fig. 8 Synthetic ground velocity time histories at the 20 grid points (Fig. 6) derived from the application of the semi-analytical method **a** fault-normal component, **b** fault-parallel component and **c** vertical component of ground motion. Synthetics refer to the M5.8 earthquake scenario on the Xanthi fault
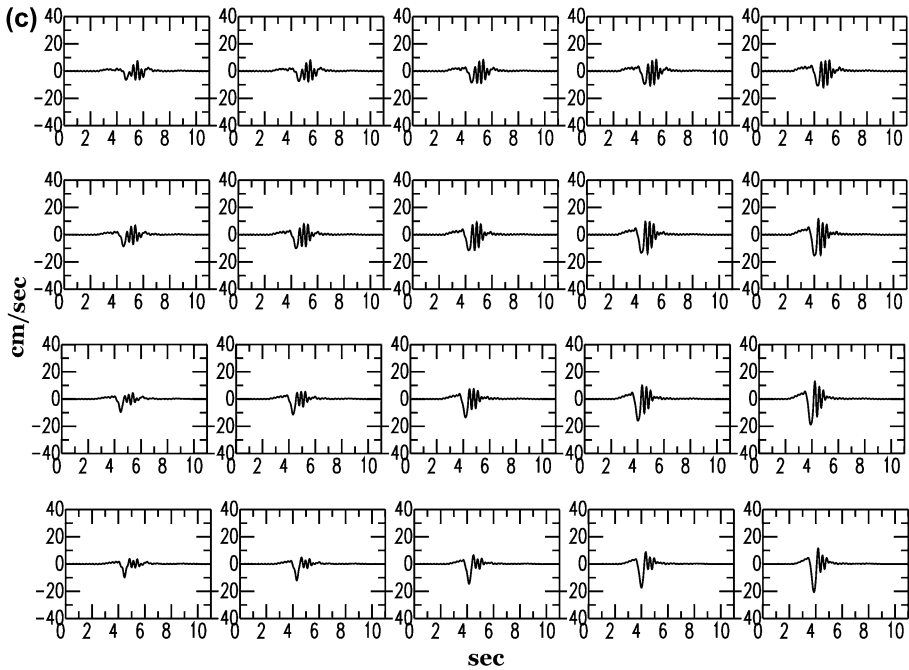
Fig. 8 continued

Table 5 1-D velocity model used for the calculation of theoretical Green's functions (modified from Papazachos 1998)

Top of layer (km)	V_P (km/s)	V_S (km/s)	ρ (g/cm^3)
0.0	2.25	1.29	2.40
1.0	6.10	3.49	2.60
3.0	6.12	3.50	2.60
5.0	6.13	3.50	2.60
7.0	6.14	3.51	2.60
9.0	6.15	3.51	2.60
11.0	6.19	3.54	2.60
13.0	6.23	3.56	2.60
15.0	6.30	3.60	2.90
17.0	6.42	3.67	3.00
19.0	6.54	3.74	3.00
21.3	6.69	3.82	3.00
23.0	6.83	3.90	3.00
25.0	6.97	3.98	3.00
27.0	7.10	4.06	3.00
29.0	7.24	4.14	3.00
31.0	7.35	4.20	3.00
33.0	7.46	4.26	3.00
35.0	7.58	4.33	3.30
37.0	7.77	4.44	3.30

V_p velocity of primary waves, V_s velocity of shear waves, ρ density

Table 6 Values of the input parameters adopted for the finite-faults stochastic simulation of the M5.8 scenario earthquake on Xanthi fault

Parameter	Symbol	Value
Fault orientation	ϕ_1	Strike 93°
	δ_1	Dip 50°
Fault dimensions	L	Length 12 km
	w	Width 8 km
Depth of upper edge of fault	h	3.0 km
Seismic moment magnitude	M_w	5.8
Stress parameter	Stress	56 bars
Number of subfaults (along strike × along dip)	$N_L \times N_W$	12×8
Subfault including the hypocentre	i_0, j_0	6, 7
Crustal shear-wave velocity	β	3.4 km/s
Crustal density at source depth	ρ	2.7 g/cm^3
Geometric spreading as a function of distance, R (km)		1/R
Source duration	T_S	1/f_{0s}, f_{0s} being the subfault corner frequency
Path duration ($T_P = bR$)	T_P	b = 0, R < 10 km; b = 0.16, $10 \leq R \leq 70$ km (Atkinson and Boore, 1995)
Anelastic attenuation model, Q(f) = Q_0*f**eta	Q_0	88.0
	η	0.9
Kappa	κ_0	0.035 s
Site amplification empirical factors	A(f)	Klimis et al. (2006)

Fig. 9 Synthetic ground velocity time histories at the 20 grid points derived from the application of the stochastic, finite-faults strong ground motion simulation method to study the M5.8 earthquake scenario on the Xanthi fault
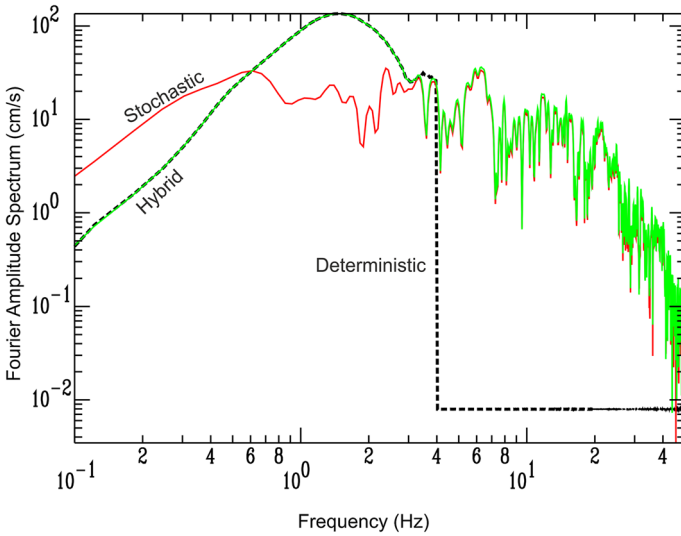
Fig. 10 An example of the synthesis in the frequency domain showing the Fourier amplitude spectra of acceleration at one of the central grid points. *Red colour* is used for the stochastically determined spectrum, while black is used for the result of the semi-analytical approach. The hybrid spectrum (*green colour*) follows the semi-analytical one up to approximately 3.2 Hz and beyond this frequency it is shaped by the results of the stochastic method. The frequency of 3.2 Hz is where the two independent spectra present the maximum convergence in their amplitudes and phases
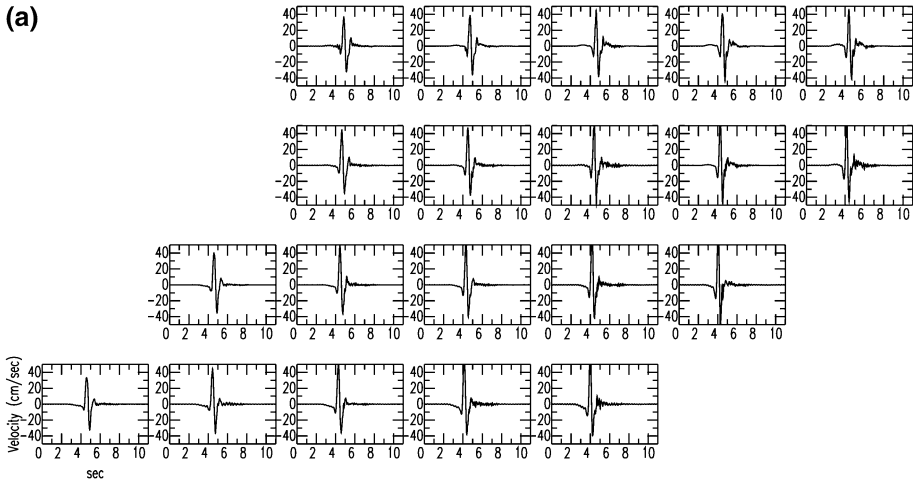
Fig. 11 Hybrid synthetics at the 20 grid points derived from merging the simulation results of COMPSYN and EXSIM: **a** velocity time histories, **b** acceleration time histories. Results refer to the earthquake scenario of M5.8 on the Xanthi fault

(b)
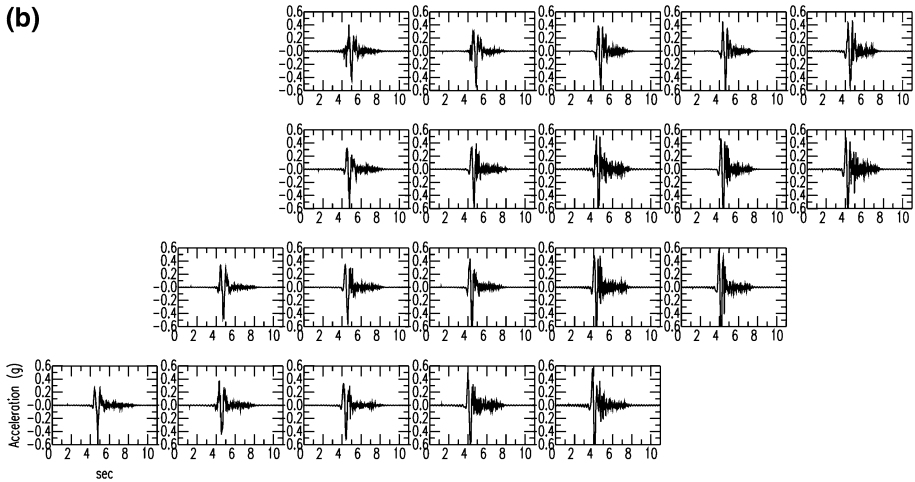
Fig. 11 continued

Finally, the deterministic and stochastic time histories, derived at each grid point, were combined to a synthetic hybrid. Merging of the independently computed ground motions was done in the frequency domain, following the approach of Mai and Beroza (2003). We used a frequency window of 3.0 ± 1.0 Hz, within which we sought for the discrete frequency where the two spectra have best convergence, both in terms of spectral amplitude and phase. An example of this procedure for one of the central grid points is presented in Fig. 10. The hybrid Fourier spectrum is then inversely transformed to compute hybrid synthetic time histories.

Our final hybrid time-series at the 20 grid points are shown in Fig. 11 both for the ground velocity and the ground acceleration. One thing to note is that these synthetics correspond to the fault-normal component of ground motion, which according to the results of the semi-analytical approach, is the one to experience stronger ground shaking from the examined earthquake scenario. The strong source effect is the reason why the results of the two methodologies are so different in the low frequencies (e.g., Fig. 10), since this effect is taken into account in COMPSYN but not in EXSIM. Hybrid time-series were produced for the fault parallel and the geometric mean of the two horizontal components of ground motion as well, but are not shown here for reasons of space economy. In all cases the input from the stochastic method remained the same (random horizontal component), but the low-frequency input varied according to the component-specific results of COMPSYN.

5 Conclusions: discussion

Suggesting realistic design ground motions in areas of sparse seismological data remains one of the most troublesome topics amongst seismologists and engineers. In this study, we present an approach to reach accurate estimates of strong ground motion. Our case study is the city of Xanthi in northern Greece, which is situated in a, presently, low seismicity region, but also at the proximity of the most prominent seismotectonic and morphological feature of northern Greece, the Kavala–Xanthi–Komotini fault. Our approach seeks to exploit all the available and most up-to-date geological and seismological data. We re-

assess the hazard of the study area through a probabilistic approach, taking into account the most recently released fault databases, and proceed to the deaggregation of the results to define realistic scenario earthquakes that we examine in a deterministic way.

We study and present synthetic velocity and acceleration time series from two scenarios: one of considerable magnitude (M6.7) at a distance of approximately 30 km from the Xanthi city centre, corresponding to a return period of 100 years and the second of moderate magnitude (M5.8) but at a very close distance to Xanthi, i.e., at 3 km, corresponding to a return period of 475 years. In the first case, derived synthetic PGA values are <0.07 g. Unless effects not encountered in the present study, e.g. site effects, have the potential to significantly amplify strong ground motion in the area, both the results of the PSHA and the deterministic analysis that we performed are well covered by the existing building code. However, when one considers the most recent geological information and assessment of the seismic potential of the close-by Xanthi fault, then synthetic ground motion can reach levels much higher than the current design levels. In several of our synthetics related to the M5.8 earthquake scenario, PGA reached values as high as 0.4 g, i.e. much higher than the current 0.16 g used in design.

The question that arises next is how simulated spectra compare to design spectra throughout the entire frequency range of engineering interest. However, our results are not directly comparable to national regulation spectra for several reasons, some of them, although not the extensive list, being:

1. PSHA spectra are UHS spectra, i.e. they comprise the combined effect of earthquakes of different distances and magnitudes that are statistically possible to affect the examined area within a certain time interval. Regulation spectra in Greece are based on the UHS concept, while our hybrid simulations correspond to a single earthquake scenario (M5.8 on the Xanthi fault), from a close to the area of interest source.
2. Regulation spectra refer to extended zones and not to specific areas (e.g., in the scale of a town), while the simulations presented herein are site-specific.
3. Regulation spectra do not account for near-source effects. In EAK 2000 (par. 5.1.2) there is the general direction that buildings should not be built next to active faults and whenever this cannot be avoided, design motion should be increased by at least 25 %. In our work, we selected appropriate tools to realistically simulate and then highlight the ground motion variability due to the fact that the examined area lies next to an active fault. We did not smooth out pertinent results but rather presented the conservative side by providing hybrid simulations for the fault-normal component, i.e. the component that shows the maximum of the near-fault effects. As shown in Fig. 8, ground motion amplitudes in this direction are 3–4 times larger compared to the fault-parallel and vertical directions.
4. Ground acceleration defined in EAK 2000 is "effective" peak ground acceleration, while the maximum of the simulated time histories is a standard peak value. Effective peak ground accelerations can be computed from peak values by multiplying the latter by a standard factor. In EAK 2000 it has not been published what this factor has been. Thus, based on the common practice in Greece, we can only assume that a factor of 0.7–0.8 is reasonable and close to what has been used on average in EAK 2000.
5. Empirical amplification factors adopted in the presented simulations (Klimis et al. 2006) correspond to $760 \leq V_{S30} \leq 1500$ m/s. Site classes in EAK 2000 are defined in a descriptive way of the surface geology and not on V_{S30} values. Thus, the correlation of our rock outcrop simulations to site class A of EAK 2000 is not straightforward and exact.

Our conclusion remains that under the assumption of an activation of the Xanthi fault, at least at the extend studied herein (M5.8), ground motion is expected to be much higher that the design motion in the near-fault area where the town of Xanthi lies. This, of course, does not mean that in case of the occurrence of such strong ground motion in reality, buildings in Xanthi will not be able to withstand the shaking. However, it does show the need of continuous updating our knowledge of the hazard in an area, especially when it comes to the design of significant structures and infrastructure.

The major shortcoming of our work is that our methods cannot be validated against real data from past earthquakes, but this is always the problem in areas similar to the one that we study. However, we chose to use tools and methods that have been extensively applied and tested in other parts of Greece, such as the stochastic simulation method. As to the application of the semi-analytical code COMPSYN, which to our knowledge has been applied only once before in Greece (Ameri et al. 2008) for "blind" ground motion predictions, as well, we do provide an example of its capability of reproducing the low-frequency part of the earthquake spectrum by applying it in the case of another significant event in the recent seismological past of Greece, which is that of the 2008 Achaia-Ilia earthquake (Supplement). Most importantly, the results that we present from the probabilistic and the deterministic approaches, at least in terms of the PGA, are consistent with each other in the intermediate frequency range where are expected to converge.

Regarding the re-estimated seismic hazard for Xanthi, our conclusions are wrapped up to the single ascertainment that existing building codes may not be adequate in cases of "extreme" or long-return period events. Although this may not be a problem for usual constructions, special attention should be paid to "significant" structures and infrastructure. The M5.8 earthquake on the Xanthi fault comprises such an example of a possibly destructive long-return-period event, as it seems to be able to cause ground motion much larger than that covered by the present building codes. And when it comes to the destructive power of an earthquake within its zone of permanent deformation (near-fault), it is well known that magnitude does not have to be large. In a seismotectonic vivid country like Greece, where the neotectonic faults are abundant, and almost everywhere, it is really hard to exclude the possibility of such destructive close-by events in any part of it. It should also be noted that exceedance of the design spectra is confirmed in most cases when the scientific community achieves to obtain near-fault ground motion records, an example from Greece being the records from the recent 2014 Cephalonia earthquakes (GEER/EERI/ATC 2014).

As a closing remark, we should note that for any further use of our results, researchers and practitioners should take into account the fact that the synthetic ground motions presented herein have been computed for rock outcrop surface conditions and include the free-surface effect.

6 Data and resources

The seismicity data were provided by the Seismological Station, Aristotle University of Thessaloniki, at (http://seismology.geo.auth.gr/ss/). Acceleration time histories used in the Supplement were provided to us by the Institute of Earthquake Engineering and Engineering Seismology (EPPO-ITSAK; http://www.itsak.gr) and the Institute of Geodynamics of the National Observatory of Athens (http://www.gein.noa.gr). Updated information on the seismic sources, used in the PSHA analysis, was provided to us by George Karakaisis

of the Department of Geophysics of the Aristotle University of Thessaloniki and Stylianos Koutrakis of the National Observatory of Athens, through personal communication.

References

Ambraseys N (2009) Earthquakes in the Mediterranean and Middle East. Cambridge University Press, Cambridge. doi:10.1017/CBO9781139195430

Ameri G, Pacor F, Cultrera G, Franceschina G (2008) Deterministic ground-motion scenarios for engineering applications: the case of Thessaloniki, Greece. Bull Seismol Soc Am 98:1289–1303. doi:10.1785/0120070114

Anderson JG, Hough SE (1984) A model for the shape of the Fourier amplitude spectrum of acceleration at high frequencies. Bull Seismol Soc Am 74:1969–1993

Atkinson GM, Boore DM (1995) Ground-motion relations for eastern North America. Bull Seismol Soc Am 85:17–30

Bazzurro P, Cornel CA (1999) Deaggregation of seismic hazard. Bull Seismol Soc Am 89:501–520

Benetatos CA, Kiratzi AA (2004) Stochastic strong ground motion simulation of intermediate depth earthquakes: the cases of the 30 May 1990 Vrancea (Romania) and of the 22 January 2002 Karpathos island (Greece) earthquakes. Soil Dyn Earthq Eng 24:1–9. doi:10.1016/j.soildyn.2003.10.003

Beresnev IA, Atkinson GM (1997) Modeling finite-fault radiation from the ωn spectrum. Bull Seismol Soc Am 87:67–84

Boore DM (1983) Stochastic simulation of high-frequency ground motions based on seismological models of the radiated spectra. Bull Seismol Soc Am 73:1865–1894

Boore DM (2003) Simulation of ground motion using the stochastic method. Pure Appl Geophys 160:635–676

Boore DM (2009) Comparing stochastic point-source and finite-source ground-motion simulations: SMSIM and EXSIM. Bull Seismol Soc Am 99:3202–3216. doi:10.1785/0120090056

Brune JN (1970) Tectonic stress and the spectra of seismic shear waves from earthquakes. J Geophys Res 75:4997–5009

Brune JN (1971) Correction. J Geophys Res 76:5002

Caputo R, Chatzipetros A, Pavlides S, Sboras S (2012) The Greek database of seismogenic sources (GreDaSS): state-of-the-art for northern Greece. Ann Geophys 55:859–894. doi:10.4401/ag-5168

Chapman MC (1995) A probabilistic approach to ground-motion selection for engineering design. Bull Seismol Soc Am 85:937–942

Cramer CH, Petersen MD (1996) Predominant seismic source distance and magnitude maps for Los Angeles, Orange, and Ventura counties, California. Bull Seismol Soc Am 86:1645–1649

Douglas J, Aochi H (2008) A survey of techniques for predicting earthquake ground motions for engineering purposes. Surv Geophys 29:187–220. doi:10.1007/s10712-008-9046-y

Feng L, Newman AV, Farmer GT, Psimoulis P, Stiros SC (2010) Energetic rupture, coseismic and post-seismic response of the 2008 MW 6.4 Achaia-Elia Earthquake in northwestern Peloponnese, Greece: an indicator of an immature transform fault zone. Geophys J Int 183:103–110. doi:10.1111/j.1365-246X.2010.04747.x

Frankel A (2013a) Comment on "Why earthquake hazard maps often fail and what to do about it" by S. Stein, R. Geller, and M. Liu. Tectonophysics 592:200–206. doi:10.1016/j.tecto.2012.11.032

Frankel A (2013b) Corrigendum to comment on "Why Earthquake Hazard Maps Often Fail and What to do About It" by S. Stein, R. Geller, and M. Liu [TECTO 592(2013) 200–206]. Tectonophysics 608:1453–1454. doi:10.1016/j.tecto.2013.08.010

Gallovič F, Zahradník J, Křížová D, Plicka V, Sokos E, Serpetsidaki A, Tselentis G-A (2009) From earthquake centroid to spatial-temporal rupture evolution: Mw 6.3 Movri Mountain earthquake, June 8, 2008, Greece. Geophys Res Lett 36:L21310. doi:10.1029/2009GL040283

Ganas A, Serpelloni E, Drakatos G, Kolligri M, Adamis I, Tsimi C, Batsi E (2009) The Mw 6.4 SW-Achaia (Western Greece) Earthquake of 8 June 2008: seismological, Field, GPS Observations, and Stress Modeling. J Earthq Eng 13:1101–1124. doi:10.1080/13632460902933899

GEER/EERI/ATC (2014) GEER Report for the 2014 Cephalonia, Greece Earthquakes [WWW Document]

Harmsen S (2001) Geographic Deaggregation of Seismic Hazard in the United States. Bull Seismol Soc Am 91:13–26. doi:10.1785/0120000007

Haslinger F, Kissling E, Ansorge J, Hatzfeld D, Papadimitriou E, Karakostas V, Makropoulos K, Kahle H-G, Peter Y (1999) 3D crustal structure from local earthquake tomography around the Gulf of Arta (Ionian region, NW Greece). Tectonophysics 304:201–218. doi:10.1016/S0040-1951(98)00298-4

Hatzidimitriou PM (1993) Attenuation of coda waves in northern Greece. Pure appl Geophys 140:63–78. doi:10.1007/BF00876871

Hatzidimitriou PM (1995) S-wave attenuation in the crust in northern Greece. Bull Seismol Soc Am 85:1381–1387

Karastathis VK, Papadopoulos GA, Novikova T, Roumelioti Z, Karmis P, Tsombos P (2010) Prediction and evaluation of nonlinear site response with potentially liquefiable layers in the area of Nafplion (Peloponnesus, Greece) for a repeat of historical earthquakes. Nat Hazards Earth Syst Sci 10:2281–2304. doi:10.5194/nhess-10-2281-2010

Kiratzi AA (2014) Mechanisms of earthquakes in Aegean. In: Beer M, Kougioumtzoglou IA, Patelli E, Siu-Kui Au I (eds) Encyclopedia of Earthquake engineering. Springer, Berlin Heidelberg, pp 1–22. doi:10.1007/978-3-642-36197-5_299-1

Kiratzi AA, Klimis N, Theodoulidis N, Margaris BN, Makra K, Christaras B, Chatzipetros A, Papathanassiou G, Savvaidis A, Pavlides SB, Roumelioti Z, Sapountzi L, Diamantis I, Lazaridis T, Petala E, Mimidis K (2013) Characterization of site conditions in Greece for realistic seismic ground motion simulations: pilot application in urban areas. Bull Geol Soc Greece XLVII:1148–1157

Klimis N, Margaris BN, Anastasiadis A, Koliopoulos P, Kirtas E (2006) Smoothed Hellenic rock site amplification factors [in Greek]. In: Proceedings of the 5th Hellenic congress of geotechnical and geoenvironmental engineering, vol 2, pp 239–246

Konstantinou KI, Melis NS, Lee S-J, Evangelidis CP, Boukouras K (2009) Rupture process and aftershocks relocation of the 8 June 2008 Mw 6.4 Earthquake in Northwest Peloponnese, Western Greece. Bull Seismol Soc Am 99:3374–3389. doi:10.1785/0120080301

Konstantinou KI, Evangelidis CP, Melis NS (2011) The 8 June 2008 Mw 6.4 Earthquake in Northwest Peloponnese, Western Greece: a case of fault reactivation in an overpressured lower crust? Bull Seismol Soc Am 101:438–445. doi:10.1785/0120100074

Koskosidi A (2014) Site-specific seismic response analysis accounting for soil profile variability in the case city of Xanthi, MSc thesis, Imperial College, London

Koukouvelas I, Pe-Piper G (1991) The Oligocene Xanthi pluton, northern Greece: a granodiorite emplaced during regional extension. J Geol Soc Lond 148:749–758. doi:10.1144/gsjgs.148.4.0749

Mai PM, Beroza GC (2003) A hybrid method for calculating near-source, broadband seismograms: application to strong motion prediction. Phys Earth Planet Inter 137:183–199. doi:10.1016/S0031-9201(03)00014-1

Margaris BN (1994) Azimuthal dependence of the seismic waves and its influence in the seismic hazard assessment in the area of Greece. Aristotle University of Thessaloniki, Thessaloniki

Margaris BN, Boore DM (1998) Determination of $\Delta\sigma$ and κ_0 from response spectra of large earthquakes in Greece. Bull Seismol Soc Am 88:170–182

Margaris B, Athanasopoulos G, Mylonakis G, Papaioannou C, Klimis N, Theodulidis N, Savvaidis A, Efthymiadou V, Stewart JP (2010a) The 8 June 2008 M w 6.5 Achaia-Elia, Greece Earthquake: source characteristics, ground motions, and ground failure. Earthq Spectra 26:399–424. doi:10.1193/1.3353626

Margaris B, Athanasopoulos G, Mylonakis G, Papaioannou C, Klimis N, Theodulidis N, Savvaidis A, Efthymiadou V, Stewart JP (2010b) Erratum: "The 8 June 2008 Mw 6.5 Achaia-Elia, Greece, Earthquake: Source Characteristics, Ground Motions, and Ground Failures" [Earthquake Spectra 26, 399–424 (2010)]. Earthq Spectra 26:1141. doi:10.1193/1.3486689

Martin L (1987) Structure et évolution récente de la Mer Égée, apports d'une étude par sismique réflexion, PhD Thèse, Université Paris 6, Villefranche-Sur-Mer

Mavroeidis GP, Papageorgiou AS (2003) A mathematical representation of near-fault ground motions. Bull Seismol Soc Am 93:1099–1131

McGuire RK (1995) Probabilistic seismic hazard analysis and design earthquakes: closing the loop. Bull Seismol Soc Am 85:1275–1284

Motazedian D, Atkinson GM (2005) Stochastic finite-fault modeling based on a dynamic corner frequency. Bull Seismol Soc Am 95:995–1010. doi:10.1785/0120030207

Mountrakis DM, Tranos MD (2004) The Kavala-Xanthi-Komotini fault (KXKF): a complicated active fault zone in Eastern Macedonia-Thrace (Northern Greece). In: Chatzipetros A, Pavlides S (eds), Proceedings of the 5th International symposium on eastern mediterranean geology, pp 857–860

Mountrakis DM, Tranos M, Papazachos C, Thomaidou E, Karagianni E, Vamvakaris D (2006) Neotectonic and seismological data concerning major active faults, and the stress regimes of Northern Greece. Geol Soc Lond Spec Publ 260:649–670. doi:10.1144/GSL.SP.2006.260.01.28

Mountrakis D, Kilias A, Pavlaki A, Fassoulas C, Thomaidou E, Papazachos C, Papaioannou C, Roumelioti Z, Benetatos C, Vamvakaris D (2012) Neotectonic study of the Western Crete and implications for seismic hazard assessment. J Virtual Explor. doi:10.3809/jvirtex.2011.00285

Olson AH, Orcutt JA, Frazier GA (1984) The discrete wavenumber/finite element method for synthetic seismograms. Geophys J R Astr Soc 77:421–460

Papadopoulos GA, Karastathis V, Kontoes C, Charalampakis M, Fokaefs A, Papoutsis I (2010) Crustal deformation associated with east Mediterranean strike–slip earthquakes: the 8 June 2008 Movri (NW Peloponnese), Greece, earthquake (Mw6.4). Tectonophysics 492:201–212. doi:10.1016/j.tecto.2010.06.012

Papaioannou CA, Papazachos BC (2000) Time-independent and time-dependent seismic hazard in Greece based on seismogenic sources. Bull Seismol Soc Am 90:22–33

Papazachos CB (1998) Crustal P- and S-velocity structure of the Serbomacedonian Massif (Northern Greece) obtained by non-linear inversion of travel times. Geophys J Int 134:25–39. doi:10.1046/j.1365-246x.1998.00558.x

Papazachos BC, Papazachou C (1997) The earthquakes of Greece [in Greek], 2nd edn. Ziti Editions, Thessaloniki

Papazachos BC, Papazachou C (2003) The earthquakes of Greece [in Greek], 2nd edn. Ziti Editions, Thessaloniki

Papazachos BC, Mountrakis DM, Papazachos CB, Tranos MD, Karakaisis GF, Savvaidis AS (2001). The faults that caused known strong earthquakes in Greece and its surroundings from the fifth century B.C. until today [in Greek]. In: Proceedings of the 2nd Panhellenic conference of earthquake engineering and engineering seismology. Thessaloniki, pp 17–26

Risk Engineering, I (1995) FRISK88M User's Manual, ver. 1.70

Roumelioti Z, Kiratzi AA, Theodulidis N (2004) Stochastic strong ground-motion simulation of the 7 September 1999 Athens (Greece) earthquake. Bull Seismol Soc Am 94:1036–1052. doi:10.1785/0120030219

Sboras S (2012) The Greek Database of Seismogenic Sources: seismotectonic implications for North Greece. University of Ferrara, Ferrara

Serpetsidaki A, Elias P, Ilieva M, Bernard P, Briole P, Deschamps A, Lambotte S, Lyon-Caen H, Sokos E, Tselentis G-A (2014) New constraints from seismology and geodesy on the Mw = 6.4 2008 Movri (Greece) earthquake: evidence for a growing strike-slip fault system. Geophys J Int 198:1373–1386. doi:10.1093/gji/ggu212

Skarlatoudis AA, Papazachos CB, Margaris BN, Theodulidis N, Papaioannou C, Kalogeras I, Scordilis EM, Karakostas V (2003) Empirical peak ground-motion predictive relations for shallow earthquakes in Greece. Bull Seismol Soc Am 93:2591–2603

Skarlatoudis AA, Papazachos CB, Margaris BN, Theodulidis N, Papaioannou C, Kalogeras I, Scordilis EM, Karakostas V (2007) Erratum to empirical peak ground-motion predictive relations for shallow earthquakes in Greece. Bull Seismol Soc Am 97:2219–2221. doi:10.1785/0120070176

Spudich P, Archuleta RJ (1987) Seismic strong motion synthetics, seismic strong motion synthetics. Elsevier, Amsterdam. doi:10.1016/B978-0-12-112251-5.50009-1

Spudich P, Xu L (2003) 85.14 Software for calculating earthquake ground motions from finite faults in vertically varying media, International Geophysics. Int Geophys. doi:10.1016/S0074-6142(03)80293-0

Stein S, Stein J (2014) Playing against nature: integrating science and economics to mitigate natural hazards in an uncertain world. Wiley, Hoboken

Stein RS, Stirling MW (2015) Seismic hazard assessment: Honing the debate testing the models, vol 96. Eos, Washington. doi:10.1029/2015EO031841

Stepp JC, Silva WJ, McGuire RK, Sewell RW (1993) Determination of earthquake design loads for a high level nuclear waste repository facility. In: Fourth DOE natural phenomena hazards mitigation conference. Lawrence Livermore National Lab., CA (USA), Atlanta, GA (USA), pp 651–657

Street RL, Herrmann RB, Nuttli OW (1975) Spectral characteristics of the Lg wave generated by Central United States Earthquakes. Geophys J Int 41:51–63. doi:10.1111/j.1365-246X.1975.tb05484.x

Theodoulidis N, Klimis N, Savvaidis A, Margaris BN, Chatzipetros AA, Papathanassiou G, Roumelioti Z, Makra K, Anthymidis M, Diamantis I, Mimidis K, Petala E, Lazaridis T, Zargli E, Kiratzi AA, Christaras B, Kontoe S, Sapountzi L (2014). Defining shallow structure properties by composing

geophysical, geological and geotechnical data for site response analysis: the case of Xanthi city (northeastern Hellas). In: Proceedings of the 2nd European conference on earthquake engineering and seismology. Istanbul, Turkey

Theodulidis N, Roumelioti Z, Panou A, Savvaidis A, Kiratzi A, Grigoriadis V, Dimitriu P, Chatzigogos T (2006) Retrospective prediction of macroseismic intensities using strong ground motion simulation: the Case of the 1978 Thessaloniki (Greece) Earthquake (M6.5). Bull Earthq Eng 4:101–130. doi:10.1007/s10518-006-9001-6

Wells DL, Coppersmith KJ (1994) New empirical relationships among magnitude, rupture length, rupture width, rupture area, and surface displacement. Bull Seismol Soc Am 84:974–1002

Zahradník J, Gallovič F (2010) Toward understanding slip inversion uncertainty and artifacts. J Geophys Res 115:B09310. doi:10.1029/2010JB007414